JMEPEG
https://doi.org/10.1007/s11665-025-11108-6


1059-9495/$19.00

ORIGINAL RESEARCH ARTICLE

# Investigating the Feasibility of Metallizing Reprocessable Vitrimeric Components through Cold Spray Technique

*Alessia Serena Perna, Antonello Astarita, Alfonso Martone, Barbara Palmieri, and Antonio Viscusi*

Submitted: 12 December 2024 / Revised: 5 February 2025 / Accepted: 28 February 2025

**Epoxy vitrimers, distinguished by their unique combination of the mechanical strength typical of thermosets with the reprocessability of thermoplastics, represent a promising class of materials for advanced technological applications. To optimize their performance in high-demand environments, surface functionalization of vitrimers and vitrimeric composites is crucial to enhance their durability and reliability in harsh conditions. This research work aims at studying the feasibility of metallising vitrimer-based components through cold spray technology. Aluminium coatings were applied under varying process parameters, inlet gas temperature ($T$ = 150 –450 °C) and standoff distance (SoD = 70 mm–100 mm), to evaluate their impact on deposition quality and substrate behaviour. The deposition processes were performed on non-reinforced vitrimeric substrates as well as on vitrimeric matrix substrates reinforced with carbon fibre fabric. The results suggest that successful metallization occurs when the substrate temperature exceeds the topology freezing transition temperature (Tv $\approx$ 170 °C), enabling the ductile behaviour necessary for effective adhesion. At $T$ = 300 °C and SoD = 100 mm, pure vitrimer coatings exhibited an average thickness of 50 $\pm$ 10 $\mu$m with minimal substrate deformation (grooves $<$ 4% of panel thickness), while lower temperatures ($T$ = 150 °C) resulted in brittle fracture and poor adhesion. Surface roughness increased from Sa = 0.15 $\pm$ 0.05 $\mu$m for uncoated substrates to Sa = 6.59 $\mu$m after coating. In contrast, composite substrates demonstrated enhanced stability due to fibre reinforcement, which constrained excessive substrate flow. At the best process conditions ($T$ = 300 °C and SoD = 100 mm), composite panels achieved homogeneous coatings with Sa = 4.513 $\mu$m. However, excessive temperatures ($T$ = 450 °C) led to substrate erosion and fibre damage in both pure vitrimer and composite panels.**

**Keywords** coatings, cold spray, composites, inorganic, polymer matrix, vitrimers

## 1. Introduction

The demand for customized materials reflects the evolving needs of industries requiring components that can withstand tougher conditions (Ref 1). Composite materials, by combining different fibres and matrices, are usefully used for customized applications due to their versatility and properties (Ref 1). The thermoset-based composites are the most widely used for high-end applications due to their mechanical strength, fibre compatibility and thermal stability (Ref 2); nevertheless, the difficulties associated with the reprocessing of thermosets and the increasing emphasis on more rigorous recycling regulations have led to a growing focus on thermoplastic matrices (Ref 3, 4). These materials, in fact, offer several advantages, including the ability to be remelted and moulded, the necessity of lower processing temperatures, and the capacity to facilitate faster and more flexible production methods (Ref 5-7).

Though high-performance thermoplastics like PEEK, PAI, and PI continue to be developed, they often struggle to meet the stringent performance benchmarks set by thermosets, especially in the most demanding conditions. In this context, a third class of polymers, known as covalent adaptable networks (CANs), is emerging as a promising alternative for use in high-performance composites (Ref 8). These materials combine the durability and strength of thermosets with unique features like flexibility, shape retention, and self-repair. Their dynamic covalent bonds enable re-moulding and recycling, similar to thermoplastics (Ref 9); among all the CANs, vitrimers are especially promising for use as polymer matrix in composites (Ref 10).

To fully leverage vitrimers and vitrimeric composites for high-demanding applications, it may be necessary to functionalize their surface to ensure performance in harsh environments. For example, while the bulk of a composite might provide structural strength, the surface may require enhanced resistance to wear, corrosion, or extreme temperatures. This is particularly

This article is an invited paper selected from presentations at the 5th International Symposium on Dynamic Response and Failure of Composite Materials, held June 17–21, 2024, in Island of Ischia, Italy, organized by Prof. Valentina Lopresto, Dr. Ilaria Papa, Prof. Michele Guida, and Prof. Antonello Astarita, University of Naples Federico II. It has been expanded from the first presentation and peer reviewed as an original paper following the standard procedure of the journal.

**Alessia Serena Perna** and **Antonello Astarita**, Department of Chemical, Materials and Production Engineering, University of Naples Federico II, P.le V. Tecchio 80, 80125 Napoli, Italy; **Alfonso Martone** and **Barbara Palmieri**, National Research Council of Italy (IPCB-CNR), Institute for Polymers, Composites and Biomaterials, 80055 Portici, Italy; and **Antonio Viscusi**, Department of Engineering and Sciences, Faculty of Technology and Innovation Sciences, Universitas Mercatorum, Piazza Mattei 10, 00186 Rome, Italy. Contact e-mail: alessiaserena.perna@unina.it.



Published online: 28 March 2025

important in aerospace components, such as turbine blades or fuselage panels, which must withstand both mechanical stresses and environmental challenges (Ref 11, 12).

Different techniques are used to functionalize the surfaces of composite materials, but several challenges remain. For example, vapour deposition techniques can create thin, uniform coatings but are costly, slow, and limited to small workpieces due to the need for vacuum chambers. These techniques also often face difficulties with adhesion to composite materials, particularly non-metallic substrates like polymers (Ref 13). Traditional thermal spray methods also present significant risks to composites, as their high temperatures can lead to thermal degradation, distortion, or damage to the polymer matrix (Ref 14). In this context, cold spray (CS) technology has emerged as an excellent alternative for metallizing composites, especially for temperature-sensitive materials such as polymers and polymer matrix composites (Ref 15, 16). Unlike thermal methods, cold spray utilizes kinetic energy instead of thermal energy to deposit metallic particles, avoiding damage of heat-sensitive substrates (Ref 17, 18). Additionally, cold spray does not require harmful chemicals or high vacuum chambers, reducing both environmental impact and operational costs (Ref 19–21).

Recent research has focused on metallizing composite surfaces using CS to achieve different metallic coatings (Ref 22–25). Works by Che et al. (Ref 26) and Sturgeon et al. (Ref 27) demonstrated successful deposition of thick metal coatings on various polymers and CFRP composites. While adhesion on thermoplastic-based materials seem guaranteed through the mechanism of mechanical interlocking (Ref 28), challenges persist with thermoset matrices, where particle adhesion is less effective, and substrate erosion is a significant issue. Several solutions were proposed in the literature with the scope to overcome this issue for thermosets (Ref 29, 30). For instance, the authors (Ref 31) investigated the development of a composite sublayer for the cold spray metallization of CFRC, with the particles embedded onto the carbon fibre-reinforced structure during the infusion process. Sun et al. proposed of using malleable Sn powder to develop an interlayer material with dendritic Cu powder to facilitate deposition on epoxy substrate (Ref 32). The results showed melting of Sn particles and severe substrate erosion at a gas temperature of more than 573 K. In this approach (Ref 33), a novel two-step process for cold spray metallization of carbon fibre-reinforced plastic was developed: the former was performed to artificially expose carbon fibres at the carbon fibre-reinforced plastic surface, in the second step, a uniform Sn coating was deposited on the eroded surface. Further research was conducted by the authors proposing a methodology that integrates the manufacturing of glass reinforced epoxy composites with functionalized surface. Particularly, the authors deposited metallic powder on the first fabric layer of the dry preform before the infusion and fixed the particles using adhesive spray, obtaining different thickness value of the metallized substrate (Ref 24). The last researches are focused differently on deriving a way to impart improved surface features on thermoplastics (TP). This approach involves the insertion of a TP layer over the thermoset substrate for fibre-reinforced composite manufacturing, as proposed by the authors (Ref 34–36).

Additionally, a biphasic Cu-epoxy sublayer was developed for metallizing CFRP structures by embedding the Cu-epoxy biphasic layer onto the CFRP surface; the cold spray deposition of diverse powders including Cu, Al, Zn and Sn was carried out (Ref 37). In this work (Ref 38), aluminium and zinc powders were mixed with tin to investigate the effect of mixing on deposition efficiency of the coating. The mixed metal powders were cold sprayed on CFRP with a low-pressure cold spray system at various conditions. It was found that the addition of aluminium or zinc resulted led to increased deposition efficiencies compared to pure tin.

Despite the growing body of research on metallizing composite materials through CS, no studies have yet investigated the metallization of vitrimer-based composites. Since vitrimers exhibit structural stability similar to thermosets at low temperatures and thermoplastic-like ductility upon heating, determining whether these materials can achieve effective metallization through cold spray without the use of interlayers or additional surface preparation techniques remains a challenge. It is essential to determine the range of parameters within which vitrimers exhibit sufficient ductility to allow the embedding of impacting particles through mechanical interlocking, without exhibiting cracking behaviour characteristic of thermosets. Furthermore, it is important to evaluate whether they can effectively retain the particles while preserving their structural integrity and functional properties. Building on these premises, the objective of this research is to experimentally evaluate the feasibility of cold spray metallization for epoxy vitrimer-based components. To this end, an epoxy vitrimer was synthesized by appropriately modifying a commercial epoxy system, and its chemical and physical properties were systematically analysed. Both pure vitrimer panels and vitrimer-based carbon fibre-reinforced panels were produced and metallized using cold spray with aluminium powders. Surface analyses were conducted to characterize the samples and evaluate the influence of the fibres on CS deposition process.

## 2. Materials and Methods

### 2.1 Production of Vitrimer-Based Substrates

The resin formulation in this study consists of a blend bisphenol A diglycidyl ether (DGEBA) epoxy resin, with tetrahydro-methyl phthalic anhydride (THMPA) functioning as the hardener, and 2,4,6-tris(dimethylaminomethyl)phenol acting as the catalyst. All materials were supplied by Huntsman Corporation. To enhance the vitrimeric properties of the epoxy system, anhydrous zinc acetate ($Zn(Ac)_2$) was introduced as a transesterification catalyst to alter the conventional resin formulation.

The formulation was prepared with a stoichiometric epoxy-to-acyl ratio of 1:1, and $Zn(Ac)_2$ was added at 10 wt.% based on the total acyl content.

The manufacturing process began with hand-mixing the epoxy resin and $Zn(Ac)_2$ powder, followed by the addition of the cross-linking anhydride. The mixture was then processed in a planetary centrifugal mixer under vacuum at room temperature. Afterwards, the amine accelerator was added, and the mixture was further mixed to ensure homogeneity.

For both the pure resin panels and the composites, the resulting mixture was cast into Teflon moulds. The composite panels were reinforced by hand-laying carbon fibre fabric (3 K T300 Twill 2 × 2, from Toray) onto the resin. The panels were then subjected to a two-stage curing process: an initial cure at 120 °C for 1 h and 30 min, followed by a secondary cure at

140 °C for 2 h. The final panels measured 100 mm × 100 mm, with a thickness of 3 mm. The manufacturing process is illustrated in Fig. 1.

### 2.2 Experimental Characterization of the Vitrimer-Based Panels

Thermogravimetric analysis (TGA) was performed using a TA Instruments Q500 to determine the thermal stability range of the polymer, following the guidelines of ASTM E1131. The measurements were carried out under an inert atmosphere by flowing nitrogen gas, with a heating rate of 10 °C/min, starting from room temperature and reaching up to 800 °C. At 600 °C, the material's weight loss was analysed.

The polymer's thermal characteristics were further examined via differential scanning calorimetry (DSC) using a Discovery DSC instrument from TA Instruments. Specimens, each weighing approximately 10 mg, were sealed in aluminium pans before analysis. The test involved two cycles of heating and cooling between 0 and 250 °C at a constant rate of 10 °C/min in a nitrogen environment. Key parameters, including the glass transition temperature (Tg) and reaction enthalpy, were obtained from the resulting DSC curves in compliance with ASTM D3418.

Dynamic mechanical analysis (DMA) was conducted using a TA Instruments Q800 in single cantilever (SC) mode. Rectangular samples with dimensions of 25 mm in length, 5.5 mm in width, and roughly 2.5 mm in thickness were analysed. The thermal behaviour of polymers was assessed over a temperature range from 30 to 180 °C, applying a heating rate of 3 °C/min, a strain amplitude of 15 $\mu$m, and a frequency of 1 Hz. The data were interpreted in line with ASTM D790, which outlines the flexural properties of reinforced and unreinforced plastics.

Creep behaviour was also evaluated using the same DMA Q800 instrument fitted with a tension film (TF) clamp. Specimens measuring 10 mm × 5.5 mm × 2 mm were tested across a temperature range of 70-245 °C, with measurements taken at 25 °C intervals. These tests were designed to monitor strain variations as the material shifted from the glassy state to the rubbery state. A constant stress of 0.1 MPa has been applied to the samples at each temperature step, for 45 min. The analysis of the creep curves enabled the determination of the topology freezing temperature (Tv) of the vitrimers, above which their mechanical behaviour exhibits a distinct transition, deviating from the characteristics of a thermoset polymer.

### 2.3 Cold Spray Deposition

The coating was produced using AlSi10Mg powders with an average particle size of 25 $\mu$m, supplied by LPW South Group, which were chosen for their compatibility with composite materials based on prior experiments conducted by the authors (Ref 39, 40). Figure 2 illustrates the particle size distribution of the powders employed in this research. A low-pressure cold spray system (DYMET 423) was utilized for the particle deposition, employing nitrogen as the carrier gas, and a cartesian robot controlling the spray gun and ensuring a consistent and repeatable deposition.

The gun traverse speed and the gas pressure values were kept constant in all the experiments. Particularly, the former was set to 1 mm/s in agreement with previous work (Ref 40); the pressure parameter was set to 6 bar, which is the standard pressure value used in low-pressure cold spray processes (Ref 41). Moreover, as reported in literature, the gas pressure has minimal influence in cold spray deposition on polymer-based materials (Ref 26, 42, 43). The powder feed rate was set to 0.2 g/s, in agreement with literature (Ref 44). A single layer of particles was applied to the composite panel using the four previously mentioned spraying conditions, resulting in metal tracks measuring 50 mm in length.

It is important to note that only the standoff distance (which is the distance between the target surface and the exit nozzle) and temperature were varied in this experimentation. Particularly, the standoff distance is of great importance because low values lead to a higher thermal exposure and a pressure force due to the powder collision during the additive growth (Ref 31, 45, 46). These results were obtained by tuning the effect of the standoff distance, transverse speed of the nozzle, and temperature of the carrier gas on the deposition efficiency (DE) in

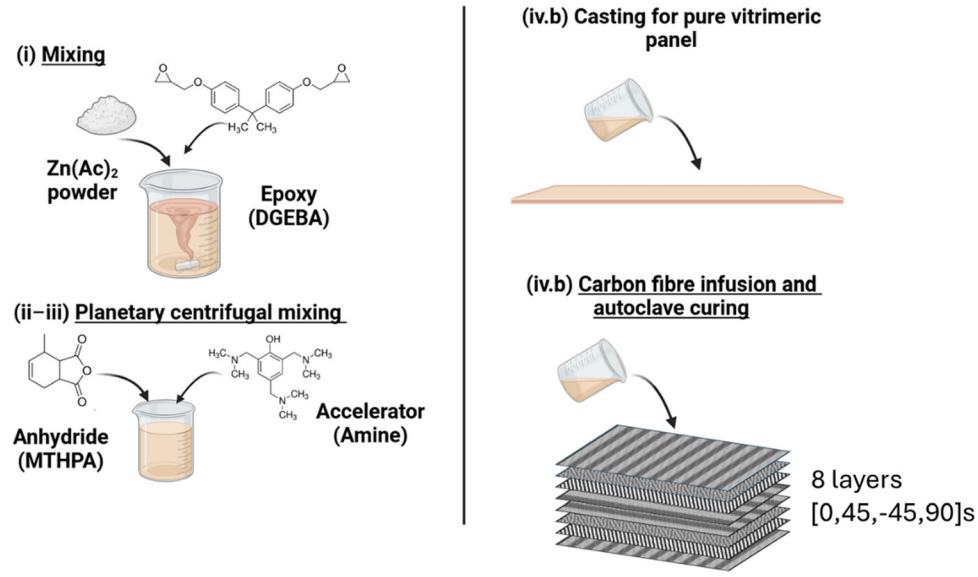


**Fig. 1** Manufacturing process of vitrimeric epoxy resin

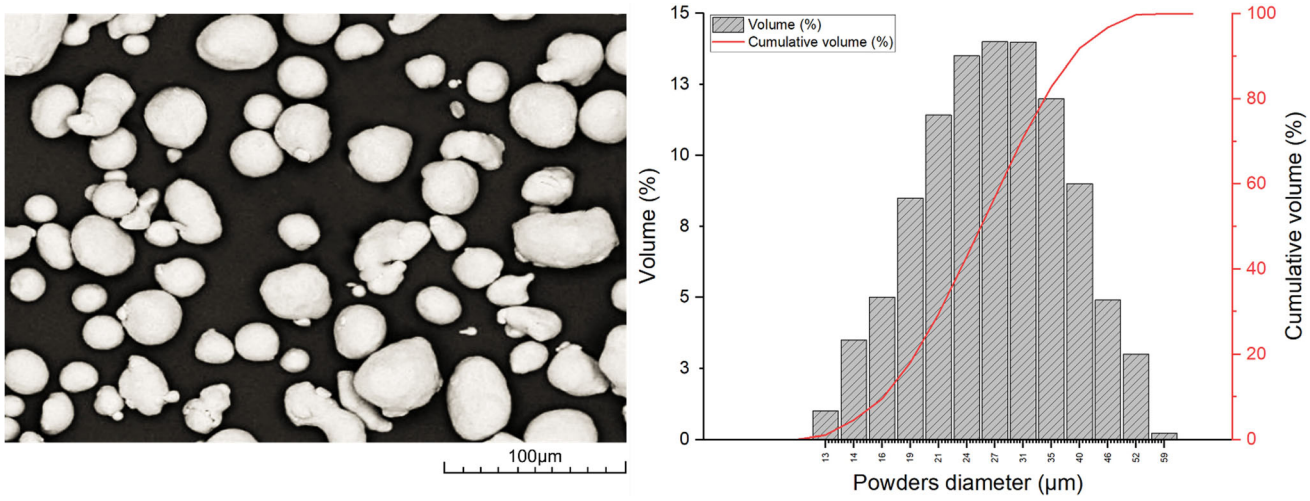


**Fig. 2** SEM micrograph and cumulative powder distribution (in volume percentage) of the AlSi10Mg powders used in this study

**Table 1 Process parameters selected for the cold spray deposition of AlSi10Mg powders on vitrimer-based substrates**

| Carrier gas | Inlet gas pressure (*P*) (bar) | Powder feed rate, g/s | Gun traverse speed, mm/s | Gas temperature (*T*), °C | Standoff distance (SoD), mm |
|---|---|---|---|---|---|
| Nitrogen | 6 | 0.2 | 1 | 150 | 70 |
| | | | | | 100 |
| | | | | 300 | 70 |
| | | | | | 100 |
| | | | | 450 | 70 |
| | | | | | 100 |

order to overcome delamination and erosion, and thus to improve DE. The authors (Ref 45) found that a good coating formation up to 400 microns can be obtained by setting a standoff distance higher than 100 mm.

Concerning the inlet gas temperature, its effects was examined by detecting the induced heating on the target surface. For this purpose, a *k*-type thermocouple was used to measure the substrate temperature as the CS parameters were varied. The measured temperature values, combined with the insights from the creep curves of the vitrimer, facilitated the selection of process parameters for studying deposition under conditions both below and above Tv. In fact, as vitrimers react to temperature variations, it is crucial to understand if the hot carrier gas used during deposition affects the substrate's response. Proper management of process parameters, such as gas temperature and standoff distance, is vital for achieving high-quality coatings. While thermoplastics required CS deposition to occur above their Tg to achieve effective deposition, vitrimer-based composites may also require consideration of their Tv. The adopted process parameters, presented in Table 1, were chosen accordingly.

To determine the optimal side of the composite panel for coating, confocal surface analyses were performed due to the differing surface characteristics resulting from contact with the Teflon mould during manufacturing, which could significantly influence the cold spray deposition, as proved in earlier studies (Ref 40). The findings from the confocal microscope analysis of the vitrimeric panel, specifically comparing the back face (in contact with the Teflon mould) and the front face, are presented in Fig. 3.

Figure 3(a) shows that the back face morphology is characterized by deep craters and grooves, significantly larger than the mean diameter of the feedstock particles. These features do not facilitate particle adhesion upon impact. Literature suggests that for effective particle interlocking, the valleys in the polymer substrate's surface texture should be comparable in size to the feedstock powder diameter (Ref 40). Analysing the arithmetical mean height (Sa) values, it is possible to assess that this back face is rougher (Sa = 3,45 ± 0,80 $\mu$m) while the front face appears smoother (Sa = 0.15 ± 0,05 $\mu$m). Similarly, for the composite substrates, the roughness of the back face is characterized by Sa = 24.192 ± 0.20 $\mu$m, while the roughness of the top face is Sa = 7.080 ± 0.70 $\mu$m. Consequently, the powders were cold sprayed onto the front face of the panel to leverage the smoother surface.

### 2.4 Panels Characterization

To assess the surface characteristics of the coated substrates, confocal analyses were performed using a laser scanning microscope Olympus OLS5100. The analyses provided topographical maps of the surface, allowing for a comprehensive evaluation of surface roughness. Measurements were taken from multiple locations on each sample to ensure accuracy and representativeness. Key roughness parameters, including average roughness (Sa) and peak-to-valley height (Sz), were calculated. In addition to roughness analysis, the morphology

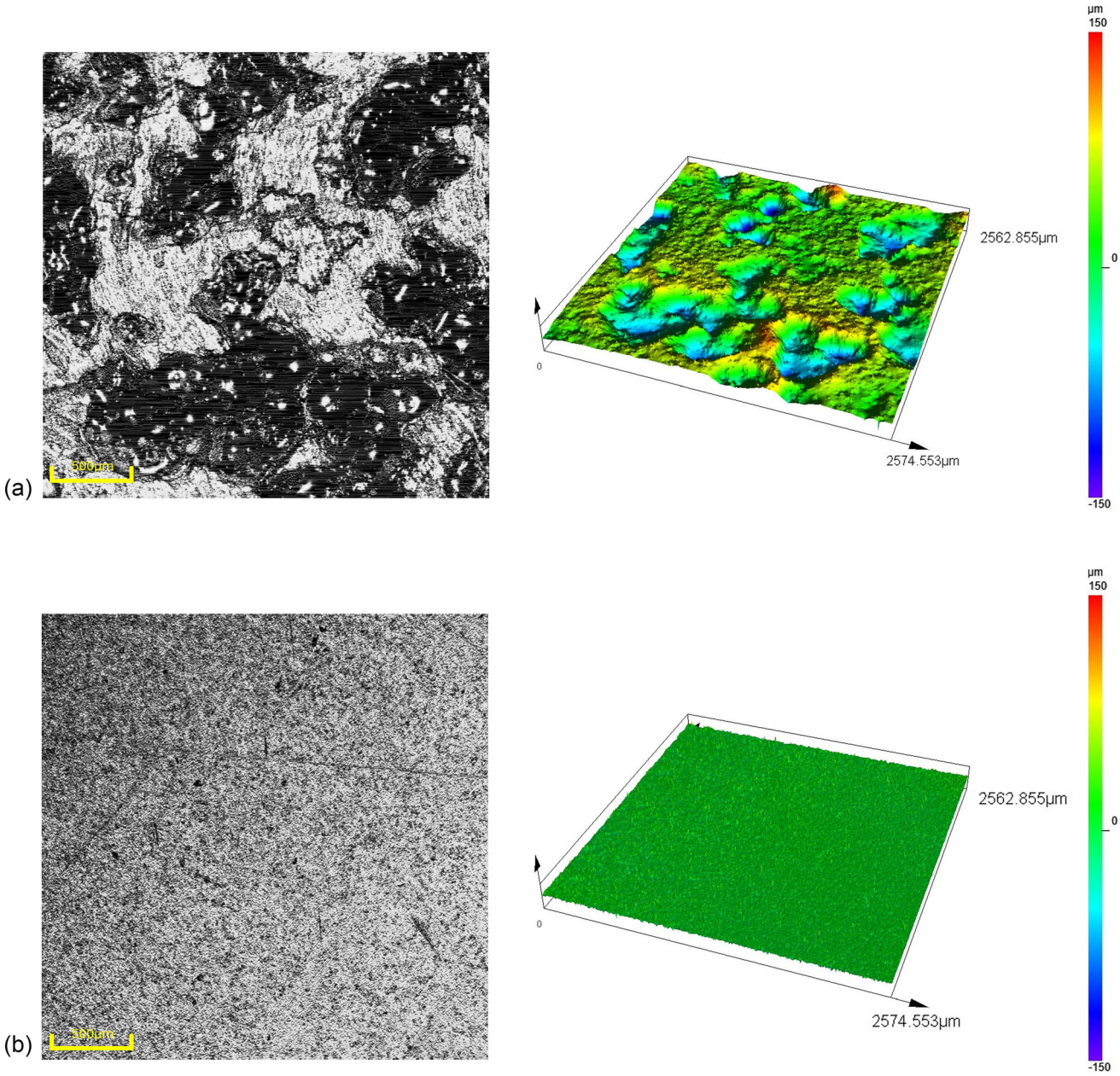


**Fig. 3** Confocal microscopy images of the bare surface prior to CS deposition: (a) a rough back surface, and (b) a smooth top surface

of the surface was thoroughly examined to assess the distribution of the coating on the vitrimeric substrates. Furthermore, Hirox microscope analyses (Hirox ST-AS) were utilized to measure the width of the coating tracks. The results obtained were then analysed and compared to enhance understanding of how the process parameters affect the characteristics of the coatings.

## 3. Results and Discussion

Figure 4 shows the TGA curves of the studied materials. The residue at 600 °C increases for the Vitrimer one due to the presence of the Zinc Acetate. The thermal degradation of vitrimeric polymer, starts at a lower temperature due to the presence of zinc acetate, which degrades at around 300 °C, as shown in Fig. 4. A 5% weight loss is found at 358 °C for the standard epoxy system; this temperature reduces when zinc acetate is added to the vitrimeric formulation as reported in Table 2.

The curing behaviour and Tg of the systems are presented in Fig. 5. The curing process is depicted in Fig. 5(a) for standard epoxy system and the vitrimer, based on the first scan of the DSC thermograms. Two exothermic peaks are observed: the first, around 140 °C, corresponds to the curing esterification reaction, while the second, between 180 and 230 °C, is associated with the homomeric ring-opening polymerization of excess epoxy groups. Zinc acetate plays a dual role by influencing the primary cross-linking reaction and activating a secondary reaction within the 180-230 °C temperature range. During the second heating ramp (Fig. 5b and d), the absence of

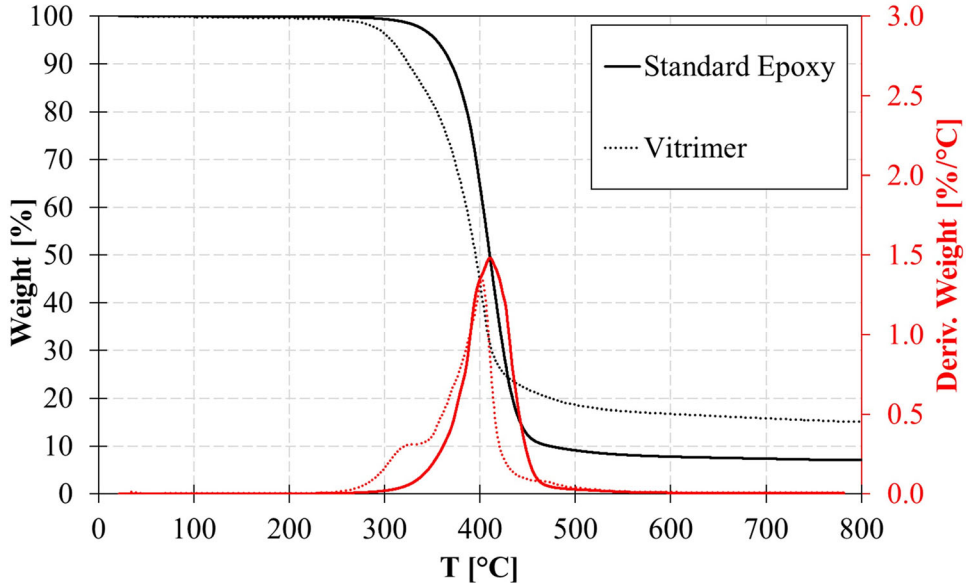


**Fig. 4** Thermogravimetric analysis (TGA) curves comparing the thermal degradation of Standard Epoxy (solid black line) and Vitrimer (dotted black line). The weight percentage (left *y*-axis) and the derivative weight loss rate (right *y*-axis, red curves) are plotted against temperature (°C). The graph highlights the distinct thermal stability and decomposition profiles of the two materials (Color figure online)

**Table 2 Results of TGA and DSC analyses**

| Description | Temperature of 5% weight loss, °C | Residue at600 °C, wt.% | Tg, DSC, °C | Reaction enthalpy, J/g | Tpeak, °C |
|---|---|---|---|---|---|
| Standard epoxy | 358 | 7.8 | 111.2 | 216.6 ± 1.2 | 130 ± 5 |
| Vitrimer | 305 | 16.8 | 94.3 | 270.3 ± 2.0 | 139 ± 2 |

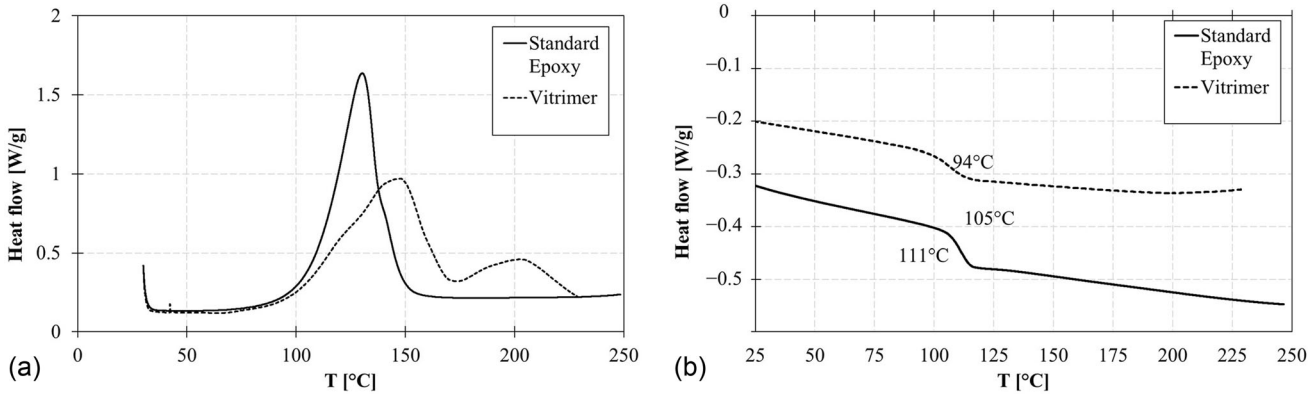


**Fig. 5** Differential scanning calorimetry (DSC) analysis comparing standard epoxy and vitrimer. (a) First heating scan showing exothermic peaks associated with the curing reaction. (b) Second heating scan illustrating the glass transition temperatures (Tg) of the fully cured systems

exothermic peaks confirms the complete conversion of the polymer. The Tg for the standard epoxy systems is measured at 111 °C. However, in the vitrimeric formulation the Tg decreases due to reduced cross-linking density. The thermal behaviour of both analysed systems, as determined by TGA and DSC experiments, is summarized in Table 2.

The viscoelastic behaviour of Epoxy standard system, with temperatures up to 180 °C, is presented in Fig. 6 and summarized in Table 3. DMA experiments were conducted within the linear viscoelastic deformation range to verify the Tg and elastic modulus of the cross-linked samples.

For the standard epoxy, the addition of zinc acetate significantly influences the material's mechanical properties. The storage modulus at room temperature increases by 31%. Similarly, the dissipation capacity, represented by the loss modulus (E″), shows a substantial enhancement with the addition of zinc acetate, increasing by + 51%. This results in an improvement in the loss factor, with the highest increase of + 16% observed in the vitrimeric formulation.

At higher temperatures (170 °C), the loss modulus of the vitrimeric system significantly surpasses that of the non-

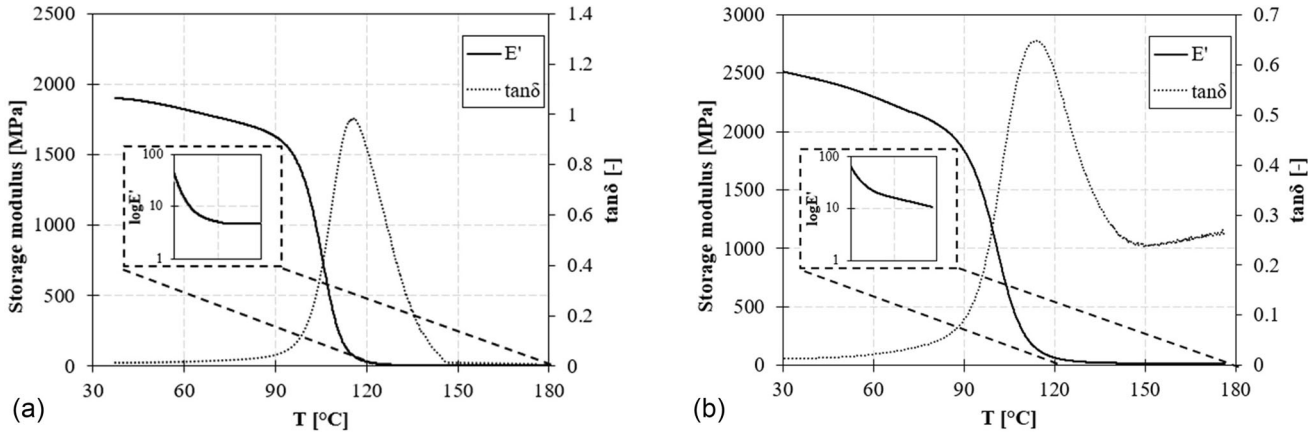


**Fig. 6** DMA curves of the (a) Standard Epoxy system and (b) Vitrimer

**Table 3 Results of DMA analysis at 35 °C and 170 °C**

| | | @35 °C | | | @170 °C | | |
|---|---|---|---|---|---|---|---|
| | $T_{g,\ DMA}$, °C | E′, MPa | E″, MPa | Tanδ (-) | E′, MPa | E″, MPa | Tanδ (-) |
| Standard epoxy | 105.6 ± 1.1 | 1899 ± 33 | 22.1 ± 0.3 | 0.0116 ± 0.0002 | 5.14 | 0.02 | 0.004 |
| Vitrimer | 101.0 ± 0.7 | 2484 ± 47 | 33.4 ± 0.3 | 0.0135 ± 0.0003 | 11.89 | 3.08 | 0.259 |

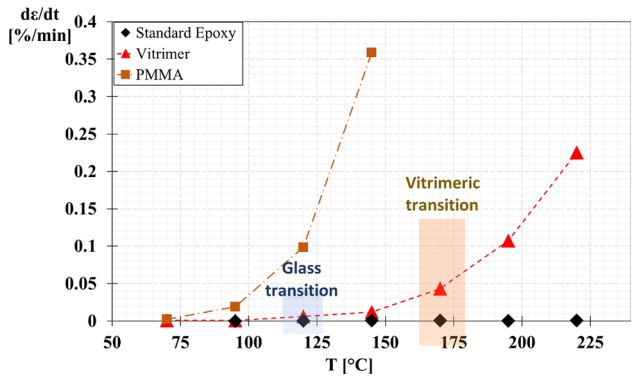


**Fig. 7** Creep curves at different temperatures of the standard epoxy (back diamond shape), vitrimeric system (dotted red line) and a standard thermoplastic system (dashed-dotted line) (Color figure online)

vitrimeric one, indicating enhanced polymer mobility induced by the zinc acetate catalyst.

Creep experiments provide clear evidence of the vitrimeric behaviour of the standard system, attributed to thermoreversible cross-linking rearrangements under constant load (Fig. 7). The non-vitrimeric formulation exhibits stable behaviour, with negligible strain increase even at elevated temperatures, demonstrating typical thermosetting properties. No molecular flow is observed, even above Tg.

In contrast, the vitrimeric formulation shows a pronounced increase in strain under constant load at temperatures exceeding Tg. The presence of zinc acetate significantly catalyses the ester interchange reaction, leading to noticeable creep behaviour at high temperatures. Above 170 °C, a substantial molecular flow is observed, corresponding to the Tv. Vitrimers undergo rapid exchange reactions above their Tv, leading to molecular rearrangement and stress relaxation (Ref 10, 47). Consequently, epoxy vitrimers can flow like a viscoelastic fluid under external forces, with viscosity decreasing according to an Arrhenius-type law as temperature rises. The higher concentration of zinc acetate in vitrimer results in a greater strain under constant load, confirming the influence of metallic ions on the system's thermoreversible properties.

Following the CS deposition, using the aforementioned process parameters, the coatings obtained on the pure vitrimer are shown in Fig. 8.

It can be observed that at lower temperatures, achieving a good CS deposition was not possible. Specifically, considering the creep curves in Fig. 7, deposition at temperature $T1$ = 150 °C is carried below the vitrimer's transition temperature. Under these conditions, the vitrimer behaves in a brittle manner, similar to a thermosetting polymer. At the shortest standoff distance (Fig. 8a), some particles adhere to the substrate, following a crack formation and filling mechanism commonly reported in the literature (Ref 48). Particles become trapped within the cracks on the polymer surface, forming a coating that is, however, uneven and weakly adhered. As the standoff distance increases (Fig. 8b), the impacting particles no longer have enough energy to crack the polymer, resulting in complete non-adhesion.

At higher temperatures ($T_2$ = 300 °C), which exceed the vitrimer's Tv, the material transitions from brittle to ductile behaviour. This transition allows the substrate to deform under particle impact, promoting the formation of a more uniform and adherent coating (Ref 49). The deposition mechanism hypothesized in this case is mechanical interlocking, which is typical of CS deposition on thermoplastic substrates. At a lower standoff distance (Fig. 8c), excessive vitrimer flow creates a depression that alters the substrate's shape in areas where the heated carrier gas contacts it. This mechanism can be furtherly observed in Hirox macrographs shown in Fig. 9(a). Compared to the average surface plane, the deposition forms a valley

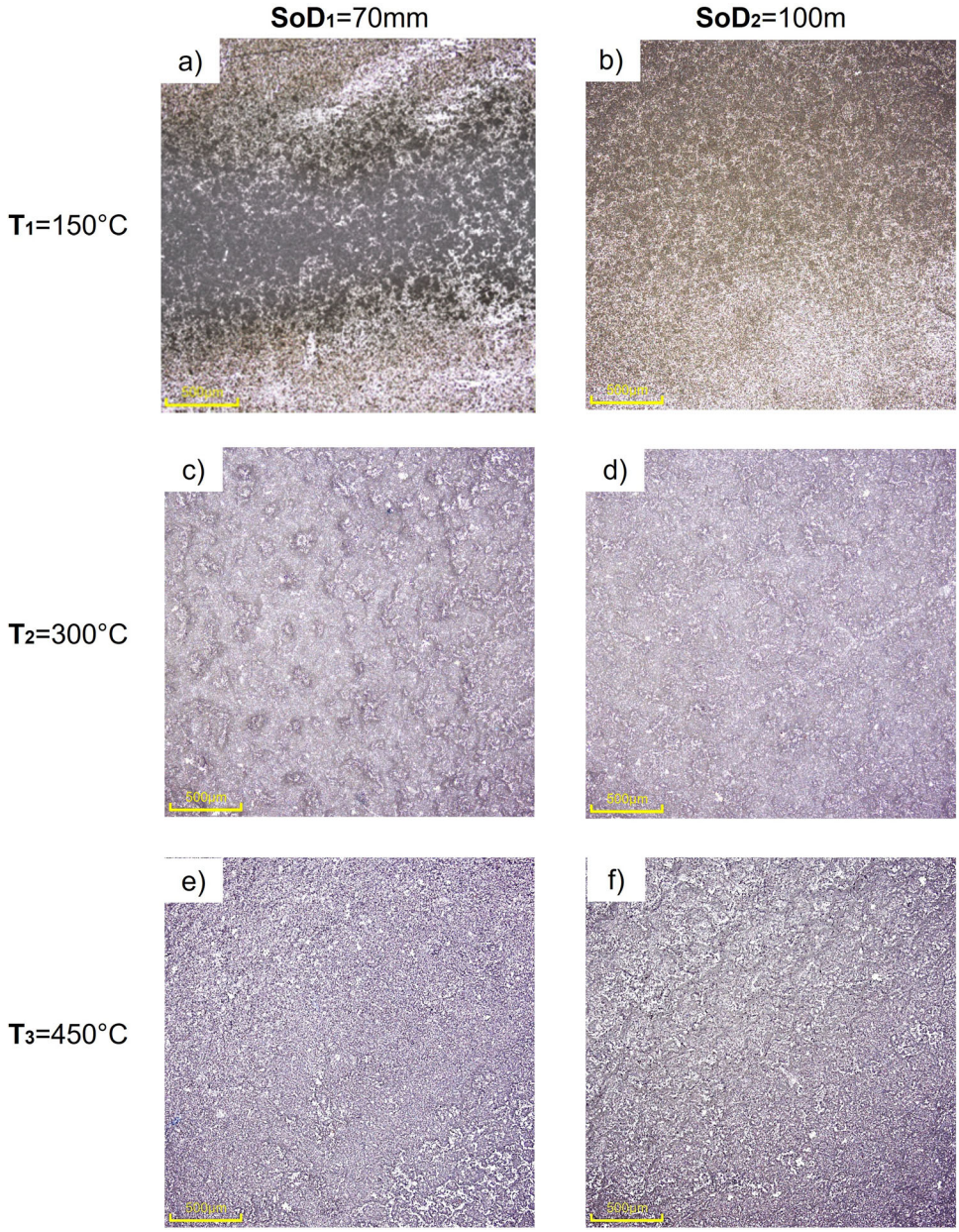


**Fig. 8** Confocal images of the pure vitrimer coated panels carried out at: (a) $T_1$ = 150 °C, $SoD_1$ = 70 mm; (b) $T_1$ = 150 °C, $SoD_2$ = 100 mm; (c) $T_2$ = 300 °C, $SoD_1$ = 70 mm; (d) $T_2$ = 300 °C, $SoD_2$ = 100 mm; (e) $T_3$ = 450 °C, $SoD_1$ = 70 mm; (f) $T_3$ = 450 °C, $SoD_2$ = 100 mm

600 microns deep (over 25% of the panel's thickness) which risks compromising mechanical properties. This effect is due to the high temperature of the impinging gas, which produces a strong shot peening effect as particles impact the softened polymer at high velocity, potentially causing substrate erosion and defects. By increasing the standoff distance (Fig. 8d), this mechanism is avoided, enabling a successful deposition. This occurs because the material flows very little, allowing high-velocity particles to bond with the polymer substrate through a mechanical interlocking mechanism (Ref 26). In this instance, the groove created by the spraying process is negligible, representing only about 4% of the panel thickness (Fig. 9b). However, as the temperature increases further, the substrate completely melts for both tested standoff distances (Fig. 8e and f). This results in an even deeper depression due to the excessively high temperature.

The Hirox microscope analysis in Fig. 9 also allows for the assessment of the track width. As the standoff distance increases, the track width decreases by 57%. This change is attributed to the shape of the carrier gas flow impacting the surface. With a greater standoff distance, more particles are present in the peripheral area of the flow, striking the substrate at non-perpendicular angles. Consequently, these particles do not have a sufficient perpendicular velocity component to exceed the critical speed, preventing them from adhering to the substrate and forming a coating.

To better understand the influence of the fibres, it is important to examine the coatings produced with the same process parameters used for the pure vitrimer on composite substrates (Fig. 10).

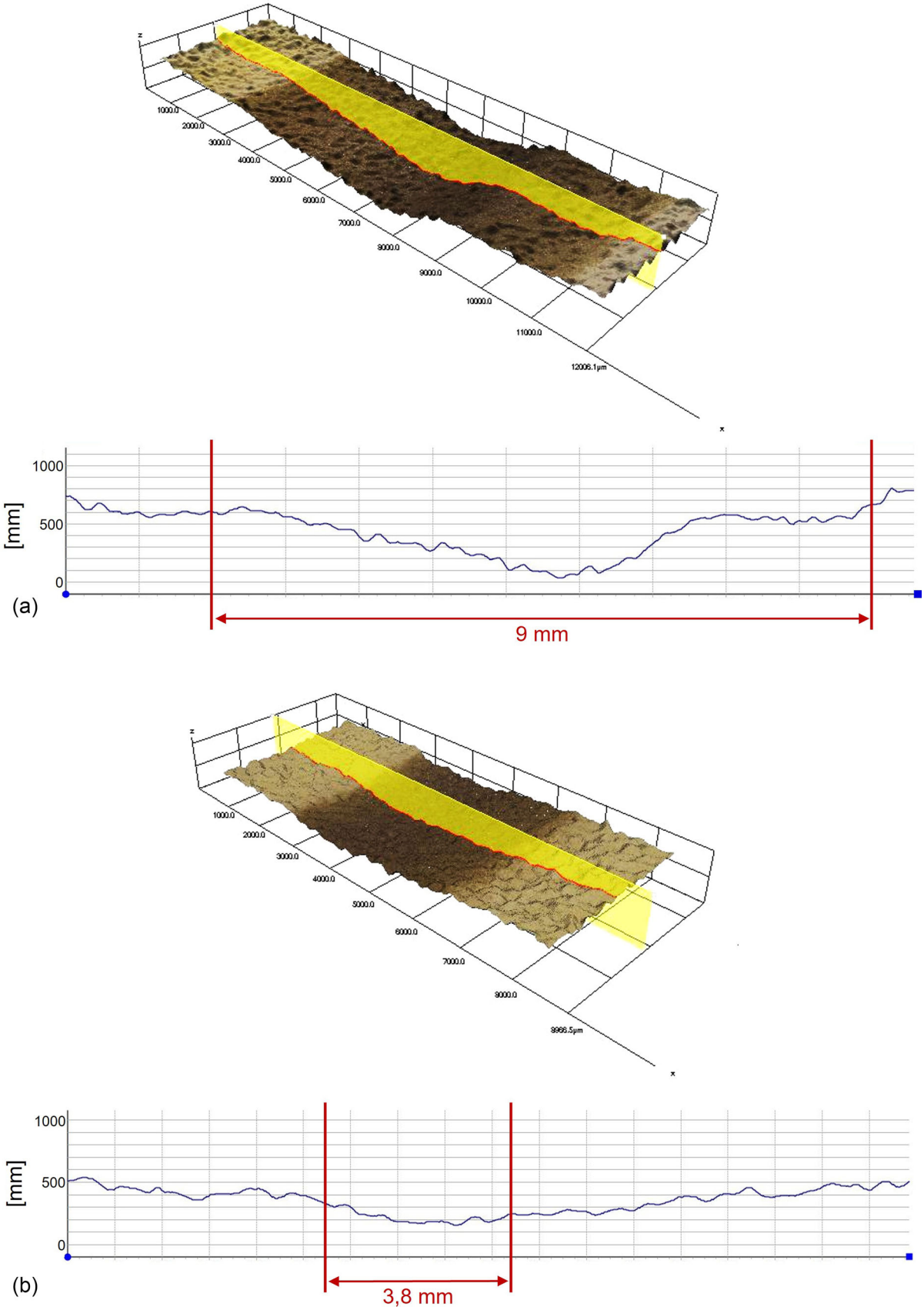


**Fig. 9** Results from Hirox observations of the pure vitrimer coated panels carried out at: (a) $T_2$ = 300 °C $SoD_1$ = 70 mm; (b) $T_2$ = 300 °C $SoD_2$ = 100 mm

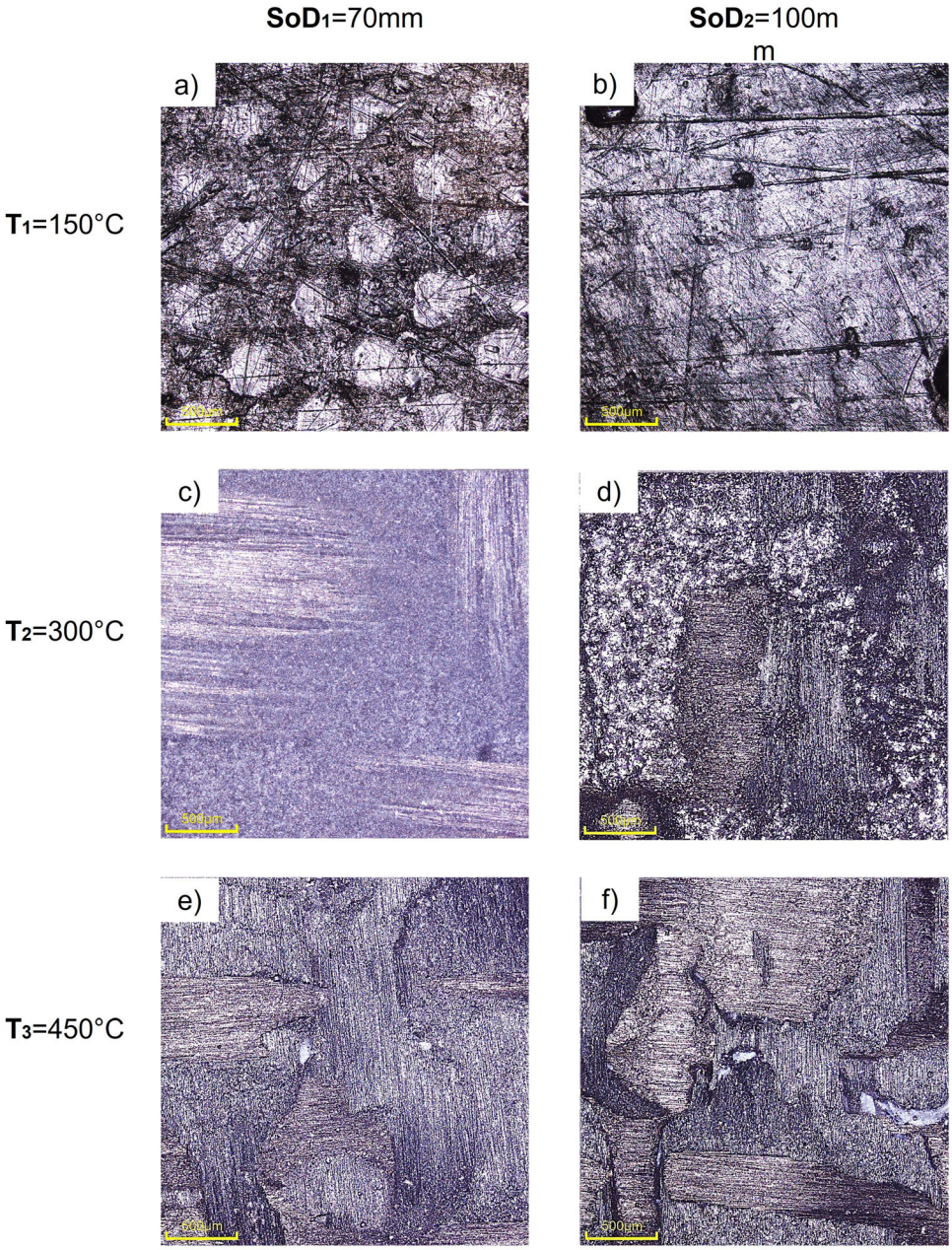


**Fig. 10** Confocal images of the composite coated panels carried out at: (a) $T_1$ = 150 °C, $SoD_1$ = 70 mm; (b) $T_1$ = 150 °C, $SoD_2$ = 100 mm; (c) $T_2$ = 300 °C, $SoD_1$ = 70 mm; (d) $T_2$ = 300 °C, $SoD_2$ = 100 mm; (e) $T_3$ = 450 °C, $SoD_1$ = 70 mm; (f) $T_3$ = 450 °C, $SoD_2$ = 100 mm

It can be observed that when the lowest temperature is selected (Fig. 10a and c), only a small number of particles can be seen on the vitrimer substrate. In fact, as assessed for the pure vitrimeric panels, this temperature is actually lower than the vitrimer's Tv; therefore, the vitrimer is able to deform enough to accommodate the impinging particles properly. As a result, cracks could form on the surface resulting in poor adhesion. On the other hand, when higher temperatures are employed and Tv is reached a rather homogeneous coating can be observed on the entire surface. Specifically, when a lower standoff value is used (Fig. 10c), the coating appears even thicker and more uniform. When the distance of the nozzle from the substrate is low, the combined effect of the ductile matrix accommodating the impacting particles and the stiffening of the panel due to the presence of fibres leads to a more homogeneous coating where the particles are able to deform and produce the coating. On the other hand, for the highest standoff value (Fig. 10d), only the areas among the fibres appear to be coated. These areas are indeed richer in vitrimeric matrix, which becomes ductile at high temperatures. The particles, for such high standoff values, do not seem to have enough energy to effectively adhere to the surface. With a further increase in temperature (Fig. 10e and f), substrate erosion is observed for both standoff distances considered. In contrast to deposition on pure vitrimer, no depressions are observed in the substrate due to the presence of the fibres, as evidenced by the Hirox analysis presented in Fig. 11.

The decrease in track width, measured using Hirox microscopy, indicates a 25% reduction as the standoff distance increases. This lesser reduction in track width, compared to the

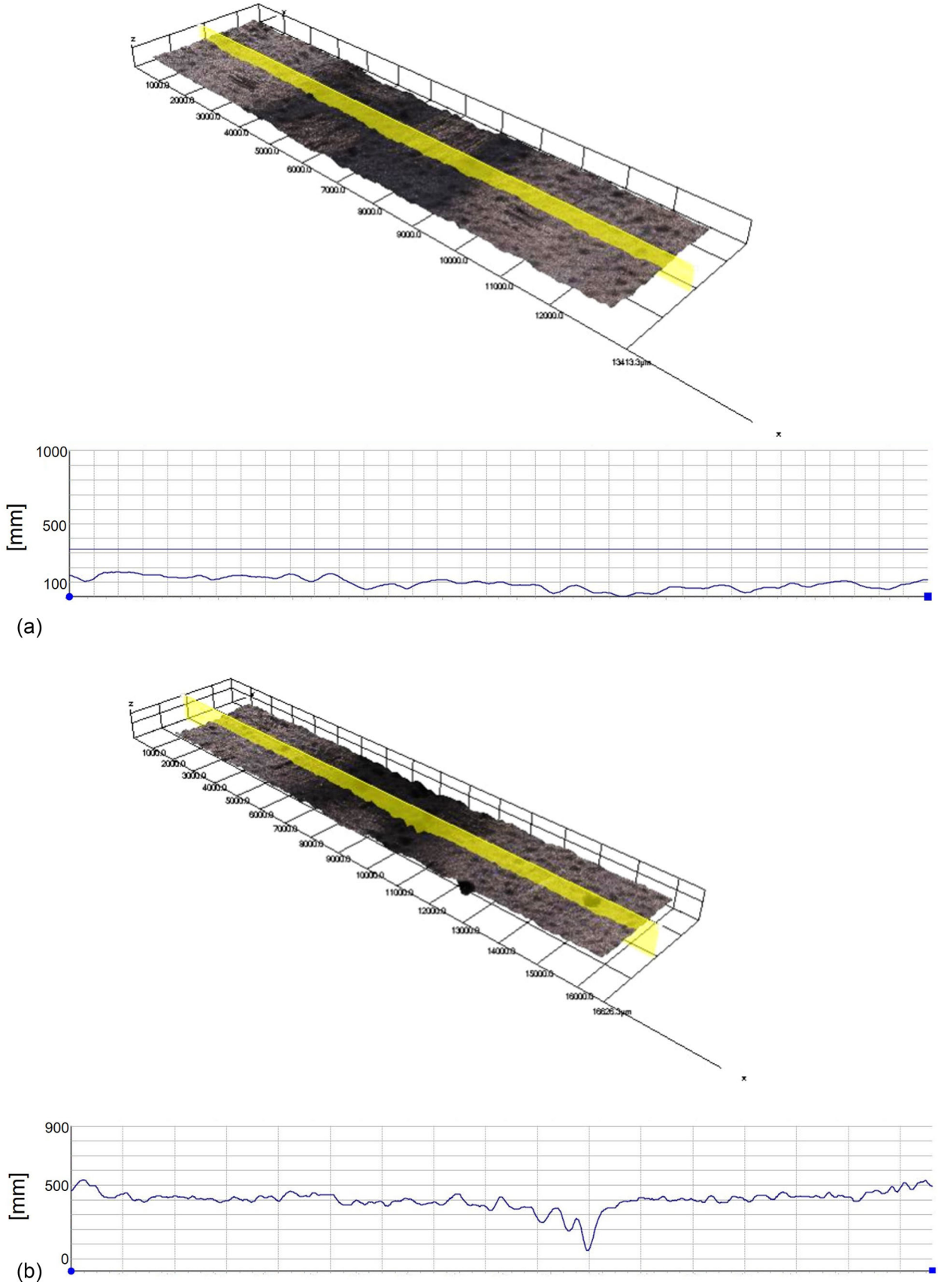


**Fig. 11** Results from Hirox observations of the composite coated panels carried out at: (a) $T_2$ = 300 °C $SoD_1$ = 70 mm; (b) $T_2$ = 300 °C $SoD_2$ = 100 mm

pure vitrimer case, may be attributed to the higher rigidity of the composite substrate.

The results from the visual inspection can be further confirmed by observing the height acquisitions of the surfaces of the coating, presented in Fig. 12, for the pure vitrimeric panels, and Fig. 13 for the composite panels. Upon analysing Fig. 13(e), it can be observed that under the most severe conditions, the fibres are exposed due to the elevated temperature attained by the panel. In the absence of the protective vitrimeric matrix, the fibres become prone to damage (Ref 50).

Table 4 presents the quantitative results for the primary surface roughness parameters, obtained from confocal analysis.

It is noticeable that for pure vitrimeric panels, all process parameters result in higher Sa values compared to uncoated surfaces presented in Fig. 3. This indicates that even in cases where the coating is not successfully produced, the surface still experiences damage and the formation of cracks, leading to an increase in the depth of the surface valleys. Under the optimal deposition conditions ($T2$ = 300 °C, SoD1 = 70 mm), the composite substrates exhibit lower roughness compared to the uncoated composite substrate. This difference is a result of the presence of the coating, which creates a more uniform surface (as shown in Fig. 10c), in contrast to the uncoated panel, which is characterized by irregularities caused by the fibres. The substantial increase in roughness observed during deposition at $T_3$ may be indicative of substrate damage. This phenomenon is consistent with findings in the literature, which suggest that a significant rise in roughness during deposition on long-fibre-reinforced materials can signal underlying substrate erosion (Ref 33).

To further examine the effect of deposition on vitrimeric substrates, Fig. 14 shows a cross section of a coating segment applied to the pure vitrimer. The measured average thickness of the coating is 50 ± 10 $\mu$m. Additionally, the deposition process has slightly modified the panel's surface morphology. Beyond the coating's penetration into the panel, the shot peening effect has caused some deformation of the substrate, making it less smooth and more irregular. Despite this, the resulting coating is uniform and continuous, with no visible distinction between the powders, which appear fused together.

We can therefore draw some conclusions regarding the deposition on vitrimer-based substrates. For both reinforced and non-reinforced panels, it is advisable to perform deposition above the vitrimer transition temperature. This enables the polymer to flow and better accommodate the impact of incoming particles. However, without fibre reinforcement, at low standoff distances, the polymer can flow excessively, forming deep valleys that damage the substrate. This effect is considerably less pronounced than in traditional thermoplastic polymers, where the material behaviour changes more linearly with temperature, as evidenced by creep curves in Fig. 7.

For deposition on pure vitrimeric panels, precise substrate temperature control is therefore essential. Fibre reinforcement alleviates this effect by constraining the polymer's flow through a mechanical restriction, allowing successful deposition even at shorter standoff distances. Conversely, at greater standoff distances, this stiffening effect can hinder deposition, as particles lack the energy to penetrate deeply and only adhere to vitrimer-rich areas where fibres lie deeper in the panel. A general outline of the deposition window for vitrimer-based substrates is shown in Fig. 15.

Examining the lower section of the sketch, it is evident that when the substrate temperature is below the vitrimer transition temperature, bonding does not occur. Instead, crack formation is promoted due to the shot peening effects caused by particles impacting the epoxy-based surface. This phenomenon applies equally to both pure polymers and fibre-reinforced variants.

As the gas process temperature increases, particle adhesion becomes feasible if the substrate temperature exceeds Tv. For this reason, the gas temperature must be carefully adjusted to a critical value, denoted Tc in Fig. 15, to ensure that the target polymer reaches the appropriate temperature for effective deposition. Notably, Tc is influenced by the standoff distance: shorter standoff distances require lower values of Tc, whereas greater distances necessitate higher values.

If the gas process temperature increases beyond this critical range, the erosion temperature ($T_{ero}$ as shown in the figure) may be reached. At this point, the substrate begins to melt, resulting in significant surface damage, such as deep depressions and grooves. Like Tc, Tero depends on the standoff distance: shorter distances lower Tero, while greater distances increase it.

These temperature-dependent mechanisms remain consistent for both pure polymers and vitrimer-based composites. In the latter case, the reinforcing fibres restrict extensive flow of the vitrimer matrix, effectively broadening the deposition temperature window and enhancing process flexibility.

## 4. Conclusions

This study investigated the feasibility of metallizing vitrimer-based composites using the CS technique, focusing on the interplay between process parameters and material behaviour. Pure vitrimer and fibre-reinforced vitrimer panels were produced and coated with aluminium powders, with inlet gas temperature and standoff distance being the primary variables. Based on the findings, the following conclusions can be drawn:

- The results confirm that vitrimer-based substrates can be effectively metallized using cold spray technology, provided the process parameters are carefully optimized. This capability introduces new opportunities for functionalizing vitrimer surfaces while avoiding thermal degradation.
- Optimizing CS deposition on vitrimer-based substrates requires precise control of substrate temperature and standoff distance. Cold spray deposition achieves the best results when conducted above the vitrimer topology freezing transition temperature (Tv ≈ 170 °C). At these temperatures, vitrimer transitions from brittle to ductile behaviour, enabling improved particle adhesion through mechanical interlocking. Excessive substrate heating or overly short standoff distances can result in substrate deformation, especially in pure vitrimer panels. Coatings produced on pure vitrimeric substrates at T = 300 °C and standoff distance SoD = 100 mm showed minimal substrate deformation (grooves < 4% of the panel thickness) and uniform coating thickness averaging 50 ± 10 $\mu$m. In contrast, temperatures below Tv resulted in brittle fracture and poor adhesion, while excessive temperatures (T = 450 °C) caused substrate erosion and deep depressions (> 25% of the panel thickness).
- In vitrimer-based composites, the presence of fibres alters the deposition dynamics compared to pure vitrimer. Fibre-reinforced vitrimer panels exhibited enhanced substrate

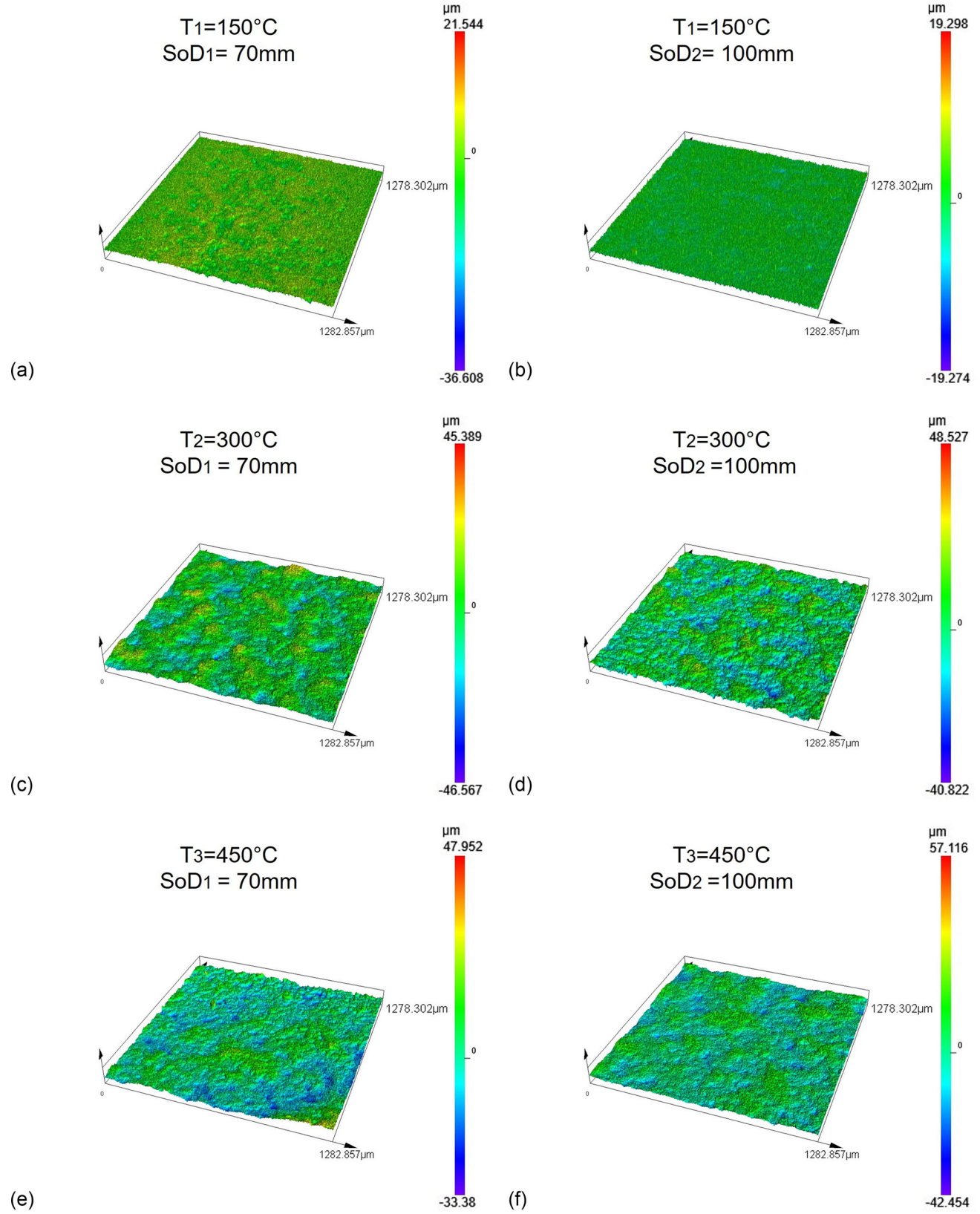


**Fig. 12** Confocal acquisition of the surface of the pure vitrimeric coated panels: (a) $T_1$ = 150 °C, $SoD_1$ = 70 mm; (b) $T_1$ = 150 °C, $SoD_2$ = 100 mm; (c) $T_2$ = 300 °C, $SoD_1$ = 70 mm; (d) $T_2$ = 300 °C, $SoD_2$ = 100 mm; (e) $T_3$ = 450 °C, $SoD_1$ = 70 mm; (f) $T_3$ = 450 °C, $SoD_2$ = 100 mm

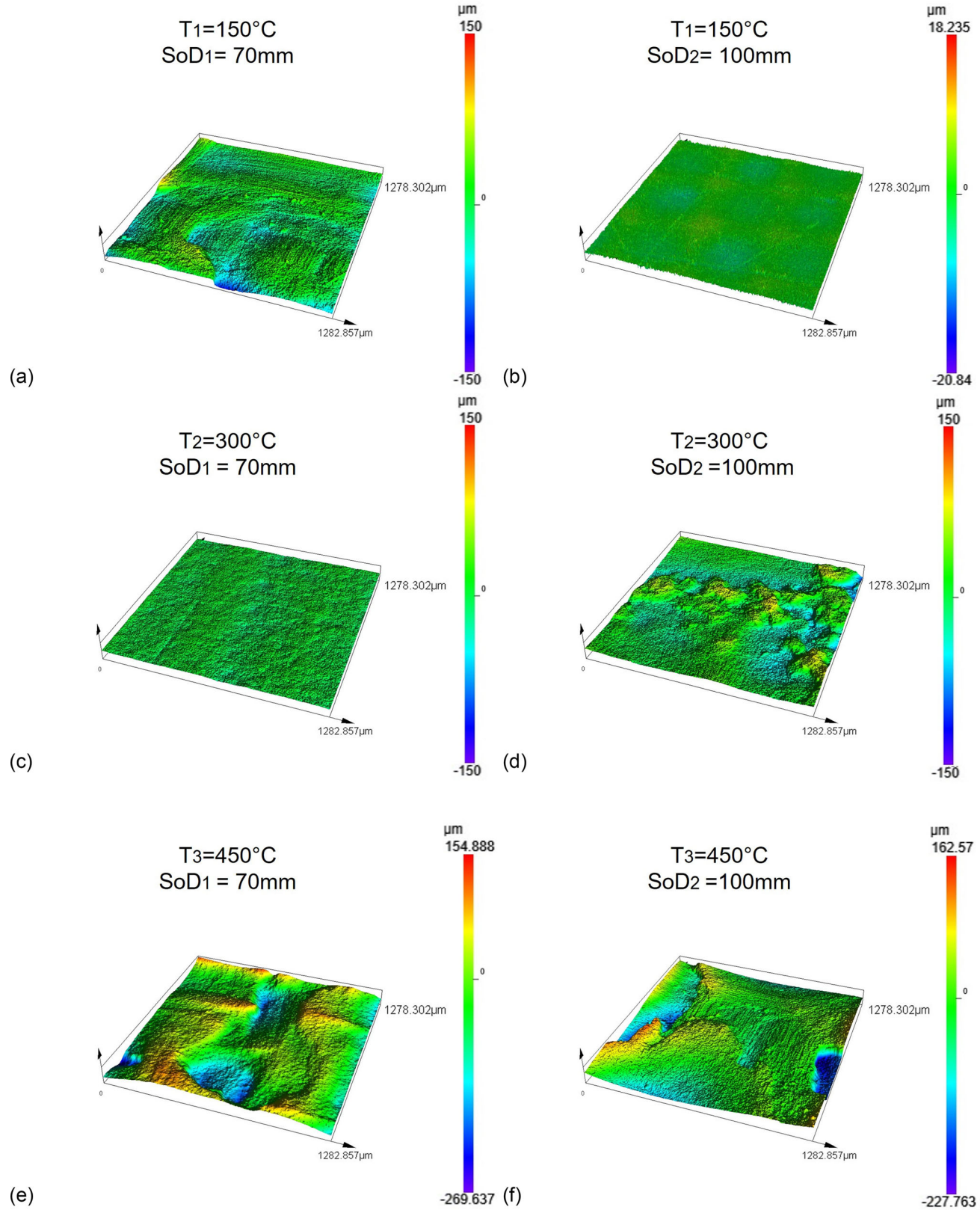


**Fig. 13** Confocal acquisition of the surface of the composite coated panels: (a) $T_1$ = 150 °C, $SoD_1$ = 70 mm; (b) $T_1$ = 150 °C, $SoD_2$ = 100 mm; (c) $T_2$ = 300 °C, $SoD_1$ = 70 mm; (d) $T_2$ = 300 °C, $SoD_2$ = 100 mm; (e) $T_3$ = 450 °C, $SoD_1$ = 70 mm; (f) $T_3$ = 450 °C, $SoD_2$ = 100 mm

**Table 4 Main Surface parameters of the coated panels**

| | $T_1$-$SoD_1$ | | $T_1$-$SoD_2$ | | $T_2$-$SoD_1$ | | $T_2$-$SoD_2$ | | $T_3$-$SoD_1$ | | $T_3$-$SoD_2$ | |
|---|---|---|---|---|---|---|---|---|---|---|---|---|
| | Sa | Sz | Sa | Sz | Sa | Sz | Sa | Sz | Sa | Sz | Sa | Sz |
| Pure Vitrimer | 2.251 | 38.178 | 1.407 | 27.421 | 6.486 | 69.659 | 6.596 | 74.318 | 5.452 | 56.990 | 5.818 | 63.079 |
| Composite | 10.595 | 99.363 | 1.633 | 30.180 | 4.513 | 54.070 | 16.743 | 148.759 | 45.807 | 327.664 | 26.940 | 324.219 |

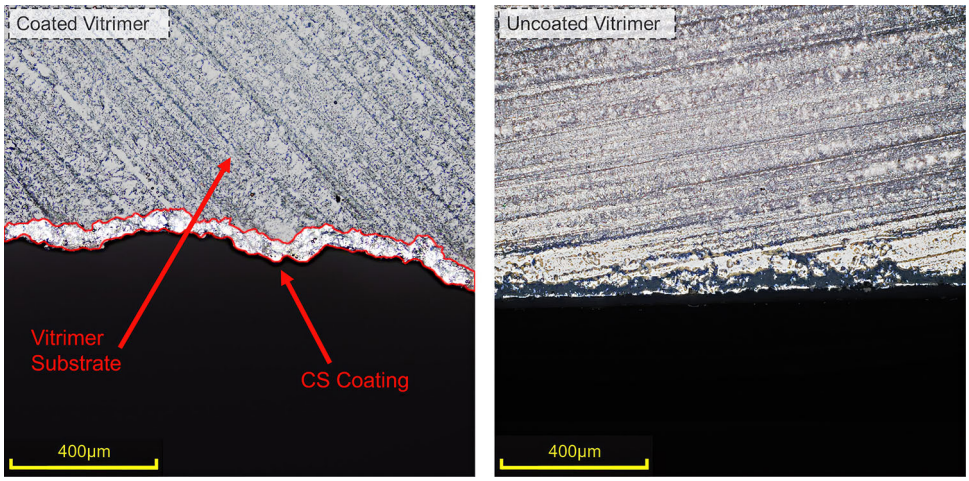


**Fig. 14** Cross section of the coating on pure vitrimer at $T_2$ = 300 °C and $SoD_2$ = 100 $\mu$m

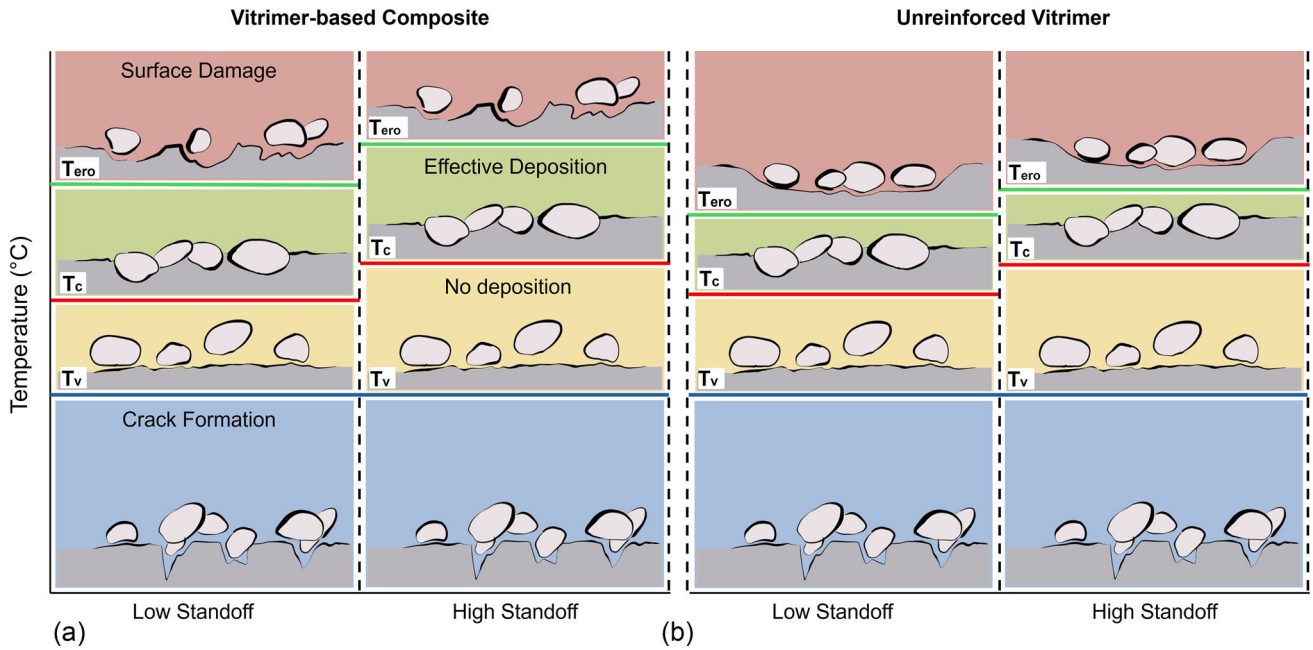


**Fig. 15** Illustrative sketch of the deposition windows for: (a) vitrimer-based composites; (b) unreinforced vitrimers

stability under cold spray conditions, reducing excessive substrate flow and deformation. At T = 300 °C and SoD = 100 mm, the depth of grooves in composite substrates was negligible compared to pure vitrimer substrates (less than 2% of panel thickness versus 25%).

- Hirox microscopy and confocal analyses revealed that for vitrimeric substrates the standoff distance plays a critical role in controlling coating width and depth. An increase in the standoff distance from SoD = 70 mm to SoD = 100 mm results in a 57% reduction in track width for pure vitrimer substrates. In contrast, composite substrates exhibit a smaller decrease (25%), owing to the greater rigidity of the substrate, which promotes the adhesion of particles that do not impact perpendicularly on the surface.

- Surface roughness increases following cold spray deposition across all tested parameters, even in cases where a complete coating is not achieved. Coated pure vitrimer panels exhibited an increase in surface roughness, with a maximum roughness value (Sa) of 6.596 $\mu$m at T = 300 °C, SoD = 100 mm, compared to 0.15 ± 0.05 $\mu$m for the uncoated substrate. For composite panels, Sa values decreased from 7.080 ± 0.70 $\mu$m to 4.513 $\mu$m under the optimal process conditions (T = 300 °C, SoD = 70 mm), due to the improved surface uniformity resulting from the presence of the coating. This indicates that the process significantly affects substrate morphology, potentially introducing cracks or deep valleys.


## Acknowledgments

This study was carried out within the "Functionally cold spRayed cOatiNgs for viTrimer composItes in lEo-space hybRid Structures (FRONTIERS)" and received funding from the Research Projects of Significant National Interest (PRIN) 2022 PNRR, project n. E53D23017120001.


## Author Contributions

Alessia Serena Perna: Conceptualization, Investigation, Data curation, Methodology, Visualization, Writing—original draft. Antonello Astarita: Project administration, Supervision; Alfonso Martone: Project administration, Supervision; Barbara Palmieri: Investigation, Data curation; Antonio Viscusi: Methodology, Investigation; Writing—review & editing.


## Funding

Open access funding provided by Università degli Studi di Napoli Federico II within the CRUI-CARE Agreement.




## References


1. I.O. Oladele, T.F. Omotosho, and A.A. Adediran, Polymer-Based Composites: An Indispensable Material for Present and Future Applications, *Int. J. Polym. Sci.*, 2020, **2020**, p 1–12
2. F.M. Monticeli, R.M. Neves, H.L. Ornaghi, and J.H.S. Almeida, A Systematic Review on High-performance Fiber-reinforced <scp>3D</Scp> Printed Thermoset Composites, *Polym. Compos.*, 2021, **42**(8), p 3702–3715
3. G. Schinner, J. Brandt, and H. Richter, Recycling Carbon-Fiber-Reinforced Thermoplastic Composites, *J. Thermoplast. Compos. Mater.Thermoplast. Compos. Mater.*, 1996, **9**, p 239–245
4. A. Bîrca, O. Gherasim, V. Grumezescu, and A.M. Grumezescu, Introduction in thermoplastic and thermosetting polymers, materials for biomedical engineering: thermoset and thermoplastic polymers, (2019)
5. S.-S. Yao, F.-L. Jin, K.Y. Rhee, D. Hui, and S.-J. Park, Recent Advances in Carbon-Fiber-Reinforced Thermoplastic Composites: A Review, *Compos. B Eng.*, 2018, **142**, p 241–250. https://doi.org/10.1016/J.COMPOSITESB.2017.12.007
6. I.Y. Chang and J.K. Lees, Recent Development in Thermoplastic Composites: A Review of Matrix Systems and Processing Methods, *J. Thermoplast. Compos. Mater.Thermoplast. Compos. Mater.*, 1988, **1**(3), p 277–296. https://doi.org/10.1177/089270578800100305
7. M. Ramesh, L. Rajeshkumar, and D. Balaji, Influence of Process Parameters on the Properties of Additively Manufactured Fiber-Reinforced Polymer Composite Materials: A Review, *J. Mater. Eng. Perform.*, 2021, **30**(7), p 4792–4807
8. Y. Zhang, L. Zhang, G. Yang, Y. Yao, X. Wei, T. Pan, J. Wu, M. Tian, and P. Yin, Recent Advances in Recyclable Thermosets and Thermoset Composites Based on Covalent Adaptable Networks, *J. Mater. Sci. Technol.*, 2021, **92**, p 75–87
9. S.-Y. Chen, S. Noor, Z. Li, Z.-H. Zhao, and C.-H. Li, Tough, Recyclable and Degradable Plastics with Multiple Functions Based on Supramolecular Covalent Adaptive Networks, *J. Mater. Chem. A Mater.*, 2024, **12**(32), p 21321–21333
10. J. Zheng, Z.M. Png, S.H. Ng, G.X. Tham, E. Ye, S.S. Goh, X.J. Loh, and Z. Li, Vitrimers: Current Research Trends and Their Emerging Applications, *Mater. Today*, 2021, **51**, p 586–625
11. M.A. Alam, H.H. Ya, S.M. Sapuan, O. Mamat, B. Parveez, M. Yusuf, F. Masood, and R.A. Ilyas, Recent Advancements in Advanced Composites for Aerospace Applications: A Review, *Advanced Composites in Aerospace Engineering Applications*, (Springer International Publishing, Cham, 2022), pp. 319–339
12. S.K. Georgantzinos, G.I. Giannopoulos, K. Stamoulis, and S. Markolefas, Composites in Aerospace and Mechanical Engineering, *Materials*, 2023, **16**(22), p 7230
13. S. Costil, E. Aubignat, C. Langlade, V. Gillet, B. Courant, P. Casari, and W. Knapp, "Organic Composite Metallization Using Low Pressure Cold Spraying," F. Azarmi, K. Balani, H. Li, T. Eden, K. Shinoda, T. Hussain, F.-L. Toma, Y.-C. Lau, and J. Veilleux, Eds., 2018, p 242–247
14. R. Lupoi and W. Oeill, Deposition of Metallic Coatings on Polymer Surfaces Using Cold Spray, *Surf. Coat. Technol.*, 2010, **205**(7), p 2167–2173. https://doi.org/10.1016/j.surfcoat.2010.08.128
15. A.S. Perna, A. Viscusi, A. Astarita, L. Boccarusso, L. Carrino, M. Durante, and R. Sansone, Manufacturing of a Metal Matrix Composite Coating on a Polymer Matrix Composite through Cold Gas Dynamic Spray Technique, *J. Mater. Eng. Perform.*, 2019, **28**(6), p 3211–3219
16. H. Che, M. Gagné, P.S.M. Rajesh, J.E. Klemberg-Sapieha, F. Sirois, D. Therriault, and S. Yue, Metallization of Carbon Fiber Reinforced Polymers for Lightning Strike Protection, *J. Mater. Eng. Perform.*, 2018, **27**(10), p 5205–5211
17. A. Astarita, L. Boccarusso, M. Durante, A. Viscusi, R. Sansone, and L. Carrino, Study of the Production of a Metallic Coating on Natural Fiber Composite Through the Cold Spray Technique, *J. Mater. Eng. Perform.*, 2018, **27**(2), p 739–750. https://doi.org/10.1007/s11665-018-3147-7
18. L. Palodhi, B. Das, and H. Singh, Effect of Particle Size and Morphology on Critical Velocity and Deformation Behavior in Cold Spraying, *J. Mater. Eng. Perform.*, 2021, **30**(11), p 8276–8288
19. S. Kumar, N.M. Chavan, and D. Srinivasa Rao, Cold Spraying: A Low Temperature Variant of Thermal Spray Techniques to Deposit Metallic Materials, *Front. Adv. Mater. Res.*, 2019, **1**(1), p 25–27
20. A. Papyrin, Cold Spray Technology, *Adv. Mater. Process.*, 2001, **159**(9), p 49–49
21. A. Viscusi, A.S. Perna, and A. Astarita, A Preliminary Study on the Sustainability of Metallization of Polymer Matrix Composites through Cold Spray, *J. Mater. Eng. Perform.*, 2023, **32**(9), p 3888–3895

22. P. Feng, M.R. Rokni, and S.R. Nutt, Depositing Aluminum onto PEKK Composites by Cold Spray, *J. Thermal Spray Technol.*, 2021, **30**(1–2), p 385–393. https://doi.org/10.1007/S11666-020-01125-3/TABLES/3
23. A. Sturgeon, B. Dunn, S. Celotto, and B. O'Neill, Cold Sprayed Coatings for Polymer Composite Substrates, *ESA SP*, 2006, **616**(1), p 1–5
24. F. Rubino, F. Tucci, V. Esperto, A.S. Perna, A. Astarita, P. Carlone, and A. Squillace, Metallization of Fiber Reinforced Composite by Surface Functionalization and Cold Spray Deposition, *Proc. Manuf.*, 2020, **47**, p 1084–1088
25. X.L. Zhou, A.F. Chen, J.C. Liu, X.K. Wu, and J.S. Zhang, Preparation of Metallic Coatings on Polymer Matrix Composites by Cold Spray, *Surf. Coat. Technol.*, 2011, **206**(1), p 132–136. https://doi.org/10.1016/j.surfcoat.2011.07.005
26. H. Che, X. Chu, P. Vo, and S. Yue, Metallization of Various Polymers by Cold Spray, *J. Therm. Spray Technol.*, 2018, **27**(1–2), p 169–178
27. A. Sturgeon, B. Dunn, S. Celotto, and W. O'Neill, Cold Sprayed Coatings for Polymer Composite Substrate, *ESA SP*, 2006, **616**(1), p 1–5
28. A.S. Perna, A. Viscusi, R. Della Gatta, and A. Astarita, Cold Spraying on Polymer-Based Composites: Understanding the Single-Particle Adhesion, *Surf. Coat. Technol.*, 2022, **447**, p 128837
29. H. Parmar, F. Tucci, P. Carlone, and T.S. Sudarshan, Metallisation of Polymers and Polymer Matrix Composites by Cold Spray: State of the Art and Research, *Perspectives*, 2021 https://doi.org/10.1080/09506608.2021.1954805
30. A. Viscusi, R. Della Gatta, F. Delloro, I. Papa, A.S. Perna, and A. Astarita, A Novel Manufacturing Route for Integrated 3D-Printed Composites and Cold-Sprayed Metallic Layer, *Mater. Manuf. Process.*, 2021, **37**, p 568–581
31. T. Zhang, E. Padayodi, I. Goda, J.-C. Sagot, and R.N. Raoelison, Development of an Epoxy-Metallic Powder Sublayer for the Cold Spray Metallization of Carbon-Fiber Reinforced Thermoset Composites, *Results Surf. Interfaces*, 2025, **18**, 100373
32. J. Sun, S. Zhou, K. Yamanaka, Y. Ichikawa, H. Saito, K. Ogawa, and A. Chiba, Thermal Effects in Sn Coating on a Carbon Fiber Reinforced Plastic by Cold Spraying, *J. Therm. Spray Technol.*, 2021, **30**(5), p 1254–1261
33. J. Sun, K. Yamanaka, C. Bernard, Y. Lei, S. Zhou, H. Lin, K. Ogawa, and A. Chiba, A Novel Two-Step Process for Enhancing Adhesion Strength of Cold-Spray Metallization of Carbon Fiber-Reinforced Plastics, *Mater. Des.*, 2025, **249**, 113568
34. H. Parmar, F. Rubino, F. Tucci, G. Rotella, P. Poza, and P. Carlone, Manufacturing and Cold Spraying of Hybrid Composites—A Path for Metallizing Thermoset Matrix Composites, *Surf. Coat. Technol.*, 2024, **489**, 131144
35. I.A. Anni, M.S. Kaminskyj, K.Z. Uddin, T.W. Bacha, N.K. Singh, J.F. Stanzione, F.M. Haas, and B. Koohbor, Thermoplastic Coating on Fiber Reinforced Polymer Composites by Cold Spray Additive Manufacturing, *Mater. Today Commun.*, 2023, **35**, 105650
36. E. Njuhovic, A. Witt, M. Kempf, F. Wolff-Fabris, S. Glöde, and V. Altstädt, Influence of the Composite Surface Structure on the Peel Strength of Metallized Carbon Fibre-Reinforced Epoxy, *Surf. Coat. Technol.*, 2013, **232**, p 319–325
37. T. Zhang, E. Padayodi, J.-C. Sagot, and R.N. Raoelison, Metallization of Carbon-Fibre Reinforced Composites via a Metal-Epoxy Biphasic Sublayer and Low-Pressure Cold Spraying, *Powder Technol.*, 2023, **426**, 118575
38. H. Che, A. Liberati, P. Vo, and S. Yue, Cold Spray of Mixed Sn-Zn and Sn-al Powders on Carbon Fiber Reinforced Polymers, *Mater. Sci. Forum*, 2018, **941**, p 1892–1897
39. R. Della Gatta, A. Viscusi, A.S. Perna, A. Caraviello, A. Astarita, R. Della Gatta, A. Viscusi, A.S. Perna, A. Caraviello, A. Astarita, R. Della Gatta, and S. Perna, Cold Spray Process for the Production of $AlSi_{10}Mg$ Coatings on Glass Fibers Reinforced Polymers, *Mater. Manuf. Process.*, 2021, **36**(1), p 106–121. https://doi.org/10.1080/10426914.2020.1813895
40. A.S. Perna, A. Viscusi, R. Della Gatta, and A. Astarita, Integrating 3D Printing of Polymer Matrix Composites and Metal Additive Layer Manufacturing: Surface Metallization of 3D Printed Composite Panels through Cold Spray Deposition of Aluminium Particles, *Int. J. Mater. Form.*, 2022, **15**(2), p 15. https://doi.org/10.1007/S12289-022-01665-9
41. R.N. Raoelison, E. Aubignat, M.-P. Planche, S. Costil, C. Langlade, and H. Liao, Low Pressure Cold Spraying under 6 Bar Pressure Deposition: Exploration of High Deposition Efficiency Solutions Using a Mathematical Modelling, *Surf. Coat. Technol.*, 2016, **302**, p 47–55
42. S. Singh, R.K.S. Raman, C.C. Berndt, and H. Singh, Influence of Cold Spray Parameters on Bonding Mechanisms: A Review, Metals (Basel), MDPI **11**(12) (2021)
43. F. Raletz, M. Vardelle, and G. Ezoo, Critical Particle Velocity under Cold Spray Conditions, *Surf. Coat. Technol.*, 2006, **201**(5), p 1942–1947
44. B. Moreno-Murguia, A.G. Mora-Garcia, H. Canales-Siller, A.L. Giraldo-Betancur, D.G. Espinosa-Arbelaez, and J. Muñoz-Saldaña, Influence of Stand-off Distance and Pressure in Copper Coatings Deposition Efficiency and Particle Velocity, *Surf. Coat. Technol.*, 2022, **430**, 127986
45. L. Lalu Khoitara, R.N. Raoelison, and S. Costil, 60% IACS Conductive Metal Coating on a Polymer Surface: Achievement of a Highly Efficient Additive Processing by Cold Spraying, *Powders*, 2022, **1**(4), p 262–272
46. R.N. Raoelison, L. Lalu Koithara, and S. Costil, Cold Spray Coating of PEEK Surface by Copper Deposition: Interfacial Adhesion at High Deposition Efficiency and Bonding Strength, *CIRP J. Manuf. Sci. Technol.*, 2021, **35**, p 63–68
47. V. Schenk, K. Labastie, M. Destarac, P. Olivier, and M. Guerre, Vitrimer Composites: Current Status and Future Challenges, *Mater. Adv.*, 2022, **3**(22), p 8012–8029
48. A. Ganesan, M. Yamada, and M. Fukumoto, Cold Spray Coating Deposition Mechanism on the Thermoplastic and Thermosetting Polymer Substrates, *J. Therm. Spray Technol.*, 2013, **22**(8), p 1275–1282
49. B. Krishnakumar, R.V.S.P. Sanka, W.H. Binder, V. Parthasarthy, S. Rana, and N. Karak, Vitrimers: Associative Dynamic Covalent Adaptive Networks in Thermoset Polymers, *Chem. Eng. J.*, 2020, **385**, 123820
50. V. Gillet, E. Aubignat, S. Costil, B. Courant, C. Langlade, P. Casari, W. Knapp, and M.P. Planche, Development of Low Pressure Cold Sprayed Copper Coatings on Carbon Fiber Reinforced Polymer (CFRP), *Surf. Coat. Technol.*, 2018, **2019**(364), p 306–316. https://doi.org/10.1016/j.surfcoat.2019.01.011